Electrostatic Deposition of Aerosol Particles Generated from an Aqueous Nanopowder Suspension on a Chemically Treated Substrate

M. Nazli Naim[1], Noor Fitrah Abu Bakar[1]*, Motoyuki Iijima[1,2], Hidehiro Kamiya[1,2], and I. Wuled Lenggoro[1,2]†

[1]*Graduate School of Bio-Applications and Systems Engineering, 2-24-16 Nakacho, Koganei, Tokyo 184-8588, Japan*
[2]*Department Chemical of Engineering, Tokyo University of Agriculture and Technology, 2-24-16 Nakacho, Koganei, Tokyo 184-8588, Japan*

Received December 1, 2009; accepted February 6, 2010; published online June 21, 2010

The state of electrostatically deposited aerosol particles from a suspension that contains TiO_2 particles on the surface of a solid substrate using electrospray was demonstrated. The particles were initially electrosterically stable in 7.5 wt % aqueous solution with a mean particle size of 50 nm. During deposition, the particles were pumped with different flow rates between 0.6 and 1.2 mL/h through a stainless steel capillary tube of 0.1 mm inner diameter. The particles were emitted at the tip of the capillary tube as an electrified liquid cone before forming into a highly charged droplet. For comparison, two types of substrate surfaces with and without chemical treatment were prepared. Atomic force microscopy (AFM) scanning and contact angle measurements showed that surface treatment increased the substrate roughness and created a hydrophilic surface. Raman analysis also showed the existence of an oxide layer and a P–O network on the treated substrate. Field emission scanning electron microscopy FE-SEM image analysis showed that more TiO_2 particles were deposited on the treated substrate than on the untreated substrate.

DOI: 10.1143/JJAP.49.06GH17

1. Introduction

Numerous electrodeposition techniques, such as electrophoretic deposition (EPD), electroplating, and cathodic sputtering, have been developed to transfer nanometer-sized ceramic particles from a liquid phase onto a desired solid surface.[1)] One of the recognized electrodeposition techniques is electrospray. Electrospray has opened a new route for realizing particle deposition in various fields, such as material technologies, microelectronics, and medical technology.[2)] This method can also be applied to a protein system and nanometer-sized particles (nanoparticles) in a liquid phase for bioapplication, and future quantum or data storage devices.[3–7)]

There are four major processes in electrospray for the formation of a nanoparticle structure, namely, (i) production of charged droplets, (ii) shrinkage of charge droplets (due to solvent evaporation) (iii) droplet-to-particle conversion, and (iv) deposition of particles to a substrate. These processes have been widely discussed in several articles.[3,8)] However, an investigation on the relationship between the deposition of aerosol particles and the surface condition of the substrate that may differ in chemical and physical structures is still a new research topic and is not well carried out.

Most solid (e.g., metal) substrates possess some finite contamination and an uneven functional group upon exposure to uncontrollable conditions, such as temperature and humidity. These phenomena may vary the adhesion force of particles and electrical properties of the substrate surface, such as resistivity and dielectric constant. As a result, the strength of the adhesion force between the particles and the substrate surface needs to be optimized to prevent or reduce particle loss during deposition.

Dry aerosol particles derived from electrospray that have been deposited on the substrate surface remain at their coordinates and are mainly due to the electrostatic force from the particle surface.[9–12)] Although various adhesion forces, such as van der Walls and capillary forces, might exist, the discussion in this study is limited to the electrostatic force aspect only. The electrostatic charge of the electrosprayed particles is obtained from the gas-phase ion on their surface that is unable to migrate during the deposition process.[11,13,14)] The electrostatic charges remaining on the surfaces of deposited particles are considered as trapped charges. The trapped charges tend to decay from the particle surface with time through the following mechanisms: by tunneling toward the conductive layer,[15–17)] decaying according to Ohm's law,[18,19,37)] and migrating through the diffusion process, whereby the diffusion current is then determined by Fick's law.[20)]

Since charge dissipation can be decayed through the above-mentioned mechanisms, a chemical treatment method with the etching of the substrate with NaOH and H_3PO_4 is proposed in this study. An oxide layer is formed and provides the substrate surface with a P–O network originating from $[PO_4]^{-3}$, which is suitable for bonding the deposited TiO_2 particles. The bonding force replaces the electrostatic force that decreases owing to charge decay or charge dissipation. It is expected that this chemical treatment method will be effective for "holding" the deposited particles on the treated surface compared with the untreated surface. The objective of this study is to investigate the effect of the chemical treatment of a solid substrate on the deposition of charged particles coming from the gas phase derived from electrosprayed droplets.

2. Experimental Methods

2.1 Material and substrate preparation

An aqueous TiO_2 suspension was prepared inside a 2.5 mL plastic (disposable) syringe using the as-received suspension (Kako). In the liquid phase, the particle size distribution was measured by dynamic light scattering (DLS) analysis (Malvern Instrument HPPS 5001). The mean diameter d_{50} of nanoparticles was 50 nm, as measured by DLS. The sources of particles in this study were the dry TiO_2 nanopowders synthesized by a gas-phase route (e.g., a flame method). The nanopowders were bead-milled with poly(carboxylate ammonium sulfate) (40% anion group) in order to form a stable (few months) TiO_2-surfactant suspension mixture. The weight ratio of TiO_2 to the surfactant (TiO_2 : surfactant)

*On leave from Faculty of Chemical Engineering, Universiti Teknologi MARA, 40450, Shah Alam, Malaysia.
†E-mail address: wuled@cc.tuat.ac.jp

was kept at 1 : 7 at 7.5 wt %. The pH values of these samples ranged from 7.99 to 8.22 at room temperature. Prior to the deposition process, the suspension was ultrasonicated for 20 min to prevent fouling on the wall surface of the container.

The zeta potential value of the liquid samples was measured using a zeta potential measurement apparatus (Nihon Rufuto). The purpose of this measurement was to determine the degree of surface charge on the surface of a suspended particle in the liquid phase. The measurement was carried out by diluting the as-received samples with ultrapure water until the concentration decreased to 0.0025 vol % from its initial concentration. By applying a DC source to the diluted samples, the average zeta potential value was measured.

2.2 Substrate treatment

An aluminum sheet of 250 mm diameter and 0.02 mm thickness was used as a substrate and grounded. Before the deposition process, the substrate was (i) submerged and stirred in NaOH (1 M) for 5 min, (ii) rinsed with ultrapure water for 5 min, and (iii) dried in an oven at 120 °C for 2 h, and (iv) the dried substrate was submerged and stirred in H_3PO_4 (0.6 M) for 10 min. Finally, the substrate was rinsed again with ultrapure water before drying in oven at 120 °C for 2 h. Then, the treated and dried substrate was kept in a desiccator before the deposition process.

2.3 Particle deposition

The deposition process was performed using an electrospray system (Shibata Scientific), which was equipped with a stainless steel capillary tube of 0.1 mm inner diameter. The particle suspension was pumped through the capillary using a pump with variable flow rates from 0.1 to 2 mL/h. A DC power supply with a positive polarity was connected to the capillary. Liquid cone-jet formation was verified visually using an optical microscope and a digital camera. To ensure stability, the electrospray current was also recorded by connecting an electrometer to the grounded electrode. Equations (1) and (2) were used to estimate the initial size of sprayed droplets and have been proposed by Hartman[21] and Ganan-Calvo,[22] respectively:

$$d_d = \left(\frac{\rho\varepsilon_0 Q^3}{\gamma K}\right)^{1/6}, \tag{1}$$

$$d_d = d_0 k_d \left(\frac{Q}{Q_0}\right)^{1/2}, \tag{2}$$

$$d_0 = (\pi^{-2}\gamma\varepsilon_0{}^2\rho^{-1}K^{-2})^{1/3}, \tag{3}$$

where d_d is the droplet size (from the current scale law), ρ is the liquid density, ε_0 is the permittivity of a vacuum ($C\,V^{-1}\,m^{-1}$), Q is the liquid flow rate ($m^3\,s^{-1}$), γ is the liquid surface tension ($N\,m^{-1}$), and K is the liquid conductivity ($S\,m^{-1}$). The constant k_d is equal to 2.9 and is assumed to be independent of liquid permittivity.

An online analysis system, which is a scanning mobility particle sizer (SMPS; TSI Model 3034) apparatus, was used to measure the size distribution of the electrosprayed aerosol particles in real time. An α-ray irradiation from the shielded Am-241 radioactive source (3.7 MBq) inside the SMPS was used to create a bipolar ionic environment.[23,24] Bipolar ions prevented the Coloumb fission of electrosprayed droplets and reduced the charge on the formed particles after the droplets shrunk and dried.[26] To suppress the formation of corona discharge, carbon dioxide was used as sheath air around the electrospray capillary.

Theoretically, the size of particles derived from sprayed droplets can be predicted using a mass balance equation. Assuming that the final particles are densed and spherical, the geometry diameter can be converted into the volume mean diameter D_v using the number frequency distribution equation $D_v = [\Sigma(\Delta N D^3{}_\rho)/N]^{1/3}$, where N is the number of particles.[27] Equation (4) can then be used to compare the final dried particle size with the size measured using the SMPS:

$$D_{v,p} = D_{v,d}\left(\frac{CM}{\rho}\right)^{1/3}. \tag{4}$$

Here, $D_{v,p}$, $D_{v,d}$, C, M, and ρ are the volume mean diameter of particles (μm), the volume of particles measured using the SMPS (μm), the precursor concentration (mol/L), the molecular weight of product particles (g/mol), and the density of product particles (g/L) respectively. By comparing the data obtained using eq. (4) with those obtained using eqs. (1) and (2), the final state of aerosol particles can be predicted before the deposition process.

Then, the electrosprayed particles were deposited on both untreated and treated grounded aluminum substrates. To maintain the deposited particles from being isolated (i.e., to inhibit the formation of adjoining structures and multilayer deposition), the substrates were rotated (50 rpm) during the deposition process. During the deposition process, unless specifically stated, the environment was controlled by conducting the experiment in a closed chamber. The chamber temperature and humidity were kept at 25 °C with a relative humidity of 70–75%. Before conducting further analysis, the substrates with deposited particles were heated in a vacuum oven at 100 °C for 2 h. Figure 1 shows the schematic diagram of the entire system used in this study.

2.4 Characterization

The morphology of the deposited particles was observed by field emission scanning electron microscopy (FE-SEM; JEOL JSM 6335F). The surfaces of the substrates were scanned at room temperature by atomic force microscopy (AFM; Digital Instrument PicoForce). Scanning speed was

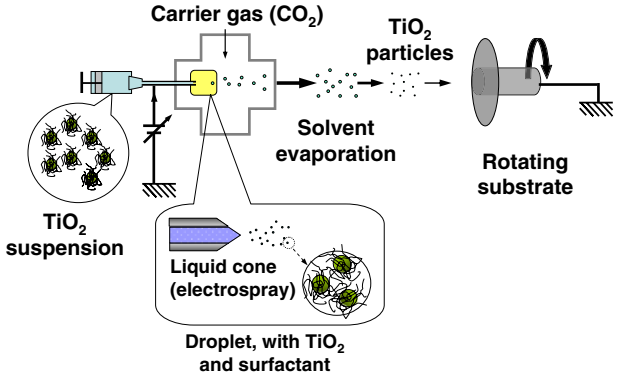

Fig. 1. (Color online) Schematic diagram of experimental apparatus for depositing aerosol particles.

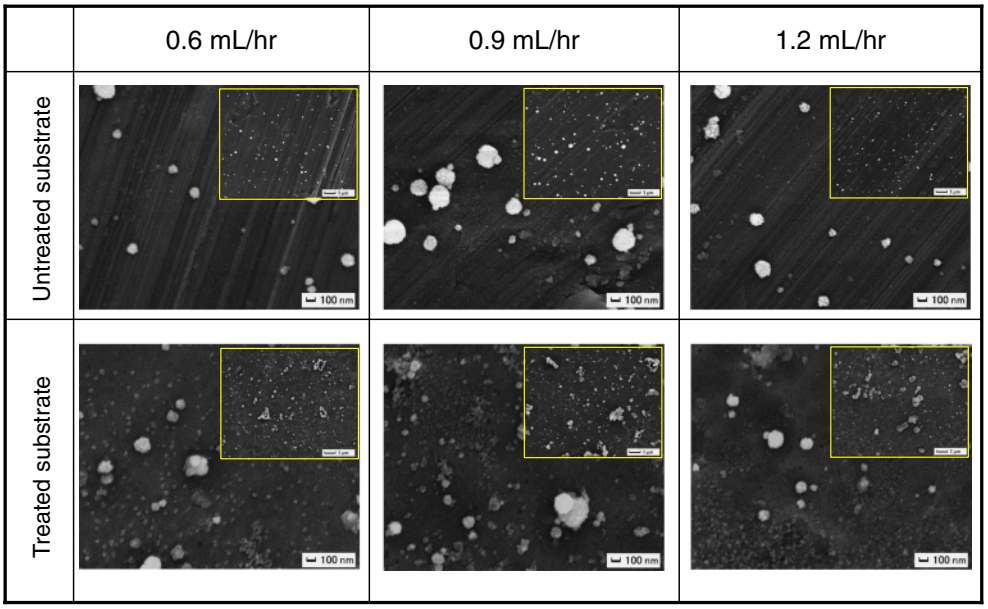

Fig. 2. (Color online) FE-SEM images of deposited particles at different flow rates on the surface of rotating substrate after 30 min of electrospray. Inset images show lower magnifications.

conducted at 0.1 Hz in a noncontact mode. Chemical properties of untreated and treated surfaces were also analyzed by Raman spectroscopy (Thermo Scientific Nicolet Almega) at room temperature. Raman spectra were generated by 532 nm He–Ne laser excitation at 17 mW. The spectral resolution of this apparatus was estimated to be less than 0.5 cm^{-1} for a slit width of 150 µm and a confocal hole diameter of 50 µm. The state of deposited particles was analyzed using image processing software (Mitani WinRoof).

3. Results and Discussion

3.1 Particle generation from electrosprayed droplets

Electrospray operation using DC at 2.7 kV and flow rates ranging from 0.6 to 1.2 mL/h was found to be sufficient for producing a cone jet under stable conditions. A stable cone jet allowed the production of monodispersed and submicrometer-sized droplets, which can also be predicted (converted) from the particle sizes measured using the online apparatus (SMPS). The size of droplets formed from the break-up of the stable cone jet was estimated using eqs. (1) and (2). Figure 2 shows the electrosprayed aerosol particles deposited on the untreated and treated substrates at different liquid supply flow rates. All figures show that the aerosol particles were aggregated (not in the state of the primary particle). Most of the size distributions of deposited particles can be estimated easily using the image analysis software because the (aggregated) particles are not adjoined owing to the rotational substrate. The untreated surfaces have a smaller number concentration of deposited particles than the treated surfaces. The details of the analysis will be discussed in §3.3.

Most of deposited (aggregate) particles were spherical with different particle size distributions when the flow rate was varied. On the other hand, Fig. 3 shows size distributions of electrosprayed particles measured in the gas phase using the SMPS. The obtained data can be considered as

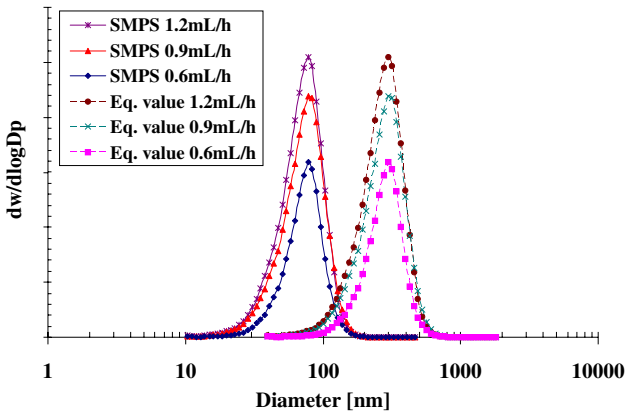

Fig. 3. (Color online) Electrosprayed particle size distributions measured using scanning mobility particle sizer (SMPS) with mean particle size of around 80 nm at various flow rates. The corresponding droplet sizes were calculated using eq. (4) with a mean size (d_{50}) of around 300 nm.

those of the shrunk aerosol particles from the electrosprayed droplets.[8] Size distributions of aerosol particles (Fig. 3) with a size range between 20 and 200 nm indicate the mean diameter d_{50} of 80 nm. The mean diameter d_{50} measured using the SMPS was slightly larger than that measured in the liquid phase by DLS analysis. This maybe attributed to the formation of electrosprayed TiO_2 particle aggregates during the electrospray process.

From the measured particle size, the droplet size can be estimated using the mass balance equation [eq. (4)]. The calculated droplet size distributions are also plotted in Fig. 3. The calculated droplet size [eq. (4)] was smaller than those estimated by Hartman [eq. (1)] or Ganan-Calvo [eq. (2)], as shown in Table I. In addition to the loss of aerosol particles due to their large size (above the micron size and the effect of gravity), the difference is probably due to the coulomb fission that occurred after the electrospray process, and also the neutralizer (Am-241) may not be

Table I. Comparison of initial droplet sizes (d_d) obtained using eqs. (1) and (2) with different supplying flow rates. Mean particle sizes measured using SMPS and eq. (4).

Flow rate (mL/h)	Mean particle size estimated using SMPS (nm)	Mean particle size estimated using eq. (4) (nm)	d_d estimated using eq. (1) (nm)	d_d, estimated using eq. (2) (nm)
0.6	80	296	1485	2007
0.9	80	296	1818	2459
1.2	80	296	2100	2839

sufficient for reducing the entire charge from the aerosol particles. In the case of highly charged droplets, shrinkage occurred owing to the evaporation of solvent and caused the droplets to approach the Rayleigh limit where they experienced an unstable coulomb fission.[8] Meanwhile, this phenomenon also indicates that the amount of charge was sufficiently high for depositing the particles on the desired substrate surface.

3.2 Surface modification of the substrate

To investigate the effect of the substrate surface condition on the charge dissipation of the deposited particles, the substrate was modified. The etching of the pure aluminum surface was performed by a dissolution–passivation technique in an alkaline medium. As mentioned in §2.2, the surface modification involved four processes. A series of three single-electron transfer reactions with hydroxide addition lead to the formation of $Al(OH)_3$.[30]

$$\begin{aligned} Al(ss) + OH^- &\rightarrow Al(OH)_{ads} + e^- \\ Al(OH)_{ads} + OH^- &\rightarrow Al(OH)_{2ads} + e^- \\ Al(OH)_{2ads} + OH^- &\rightarrow Al(OH)_{3ads} + e^- \end{aligned}$$

Here, "ss" represents a bare aluminum surface site. The final reaction step was believed to correspond to the chemical dissolution of aluminum trihydroxide in aluminum soluble species with the regeneration of a bare surface site according to the following reaction:

$$Al(OH)_3 + OH^- \rightarrow Al(OH)^-{}_4 + ss$$

$Al(OH)_3$, which accumulated on the substrate surface, was transformed to Al_2O_3 during the heating process.[31]

Al_2O_3 on the substrate surface provides an anticorrosion layer because alumina is known to be corrosion-resistant in a corrosive aqueous solution.[32] The added H_3PO_4 was expected to react only with the pure aluminum surface that was not converted to Al_2O_3. In fact, a long exposure time was also found to be useful for removing the oxide material.[33] Phosphate treatment using H_3PO_4 has been used widely as a base in paint coating.[34] The reaction of H_3PO_4 with a metal surface (e.g., aluminum) will provide a microporous layer to ensure paint adhesion. Therefore, in this study, aluminum treated with H_3PO_4 was expected to provide the P–O framework on the surface of the substrate. $[PO_4]^{-3}$ ions could provide more P–O interaction chains between the treated surface and TiO_2 particles. $[PO_4]^{-3}$ ions acting as a functional group were selected in this study because they provide the highest attraction bonding to TiO_2 particles compared with other functional groups such as hydroxyl, carboxylic acid, and sulfonic acid.[36] As a result,

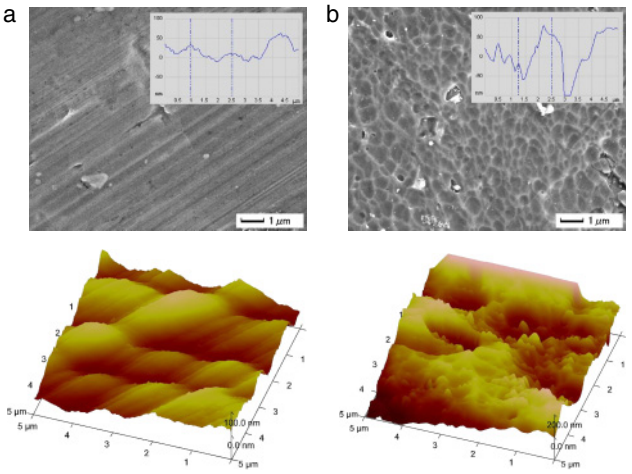

Fig. 4. (Color online) Surfaces of (a) untreated and (b) treated substrates before particle deposition observed by FE-SEM (top) and AFM (bottom). Bump depths are shown in insets.

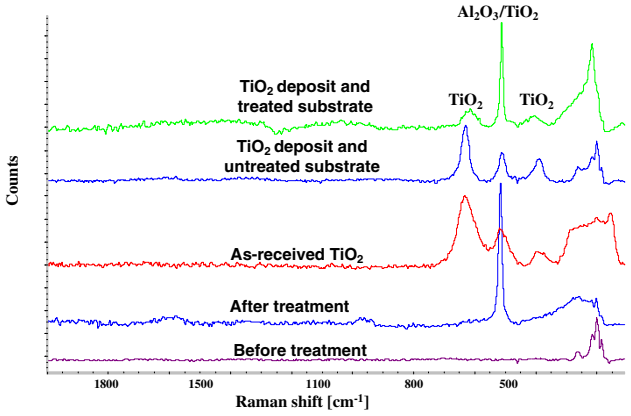

Fig. 5. (Color online) Raman spectra of untreated and treated aluminum surface before and after the deposition.

the treated substrate surface may allow more deposits due to the hydrophilic interaction induced by the P–O framework.

The formation of the oxide layer on the treated substrate surface due to the chemical treatment process reduced the contact angle from 65 to 50° between the TiO_2 suspension and the substrate. The low contact angle on the treated substrate surface was expected to provide a water layer (moisture) that induced hydrophilic interaction. The hydrophilic interaction between the surfactant (on the surfaces of TiO_2 particles) and the treated substrate surface increased the adhesion force of deposited particles when the electrostatic charges were completely dissipated. Figure 4 shows the morphology of untreated and treated substrate surfaces scanned by using AFM. This figure indicates that the chemical treatment increased the bump depth of the treated substrate surface to 50–100 nm. In addition, the chemical treatment may create a larger surface area that can entrap a high number of TiO_2 particles.

Figure 5 shows the Raman spectra of the treated and untreated substrates before and after the deposition process (with deposited particles). The treated substrate showed Al_2O_3 peaks at 540 cm^{-1}.[28] Raman analysis also verified that the deposition occurred on both types of substrates

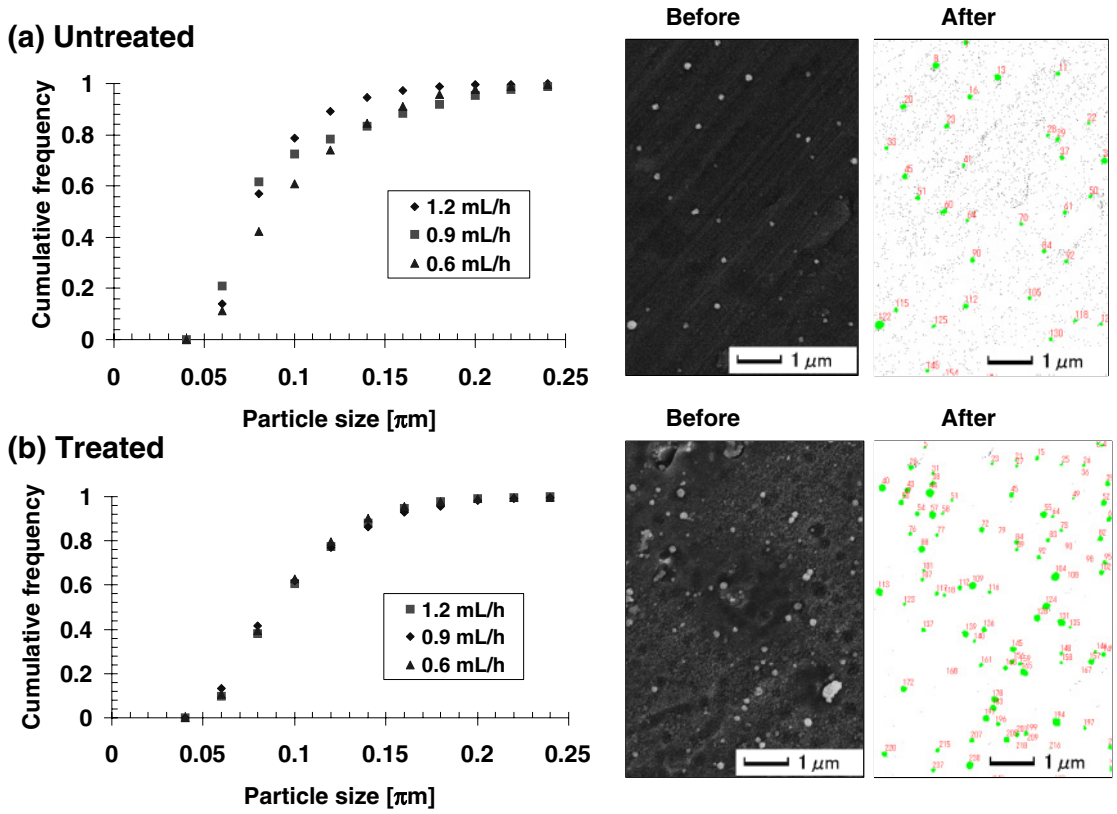

Fig. 6. (Color online) Cumulative frequencies of deposited particles on (a) untreated (b) treated substrates at different flow rates of electrospray. Images on the right side are obtained before and after the WinRoof image analysis.

because TiO_2 (anatase phase) was observed at 403, 515, and 638 cm^{-1}.[29] However, we were unable to determine the $[PO_4]^{-3}$ peaks at 284, 388, 444, and 467 cm^{-1}[35] because of the broad peak between 200 and 400 cm^{-1}.

3.3 Size distribution of deposited particles

As shown in Fig. 2, the untreated surfaces have a lower number concentration of deposited particles compared with the treated surfaces. The size of deposited (aggregate) particles analyzed using the image analysis software ranged between 50 and 250 nm. Any sizes of deposited particles beyond this range were not considered because distribution ranges were set by referring to the values of sizes measured in the gas phase using the SMPS within ±25% tolerance. Figure 6 shows the particle size distributions obtained from the FE-SEM images of the deposited particles on both substrate surfaces. Figure 6(a) shows inconsistent particle size distributions on the untreated surfaces when different flow rates of electrospray were applied. However, the same reproducible particle size distributions were obtained at different flow rates of electrospray on the treated substrate [see Fig. 6(b)]. This maybe attributed to the low charge dissipation rate of the deposited particles on the treated substrates that increased the adhesion force between TiO_2 particles and the substrate.

Figure 7 shows the FE-SEM images of particles obtained at different deposition times on the untreated and treated substrates. When the deposition time was increased from 30 to 120 min, more distinct particles were observed on the treated substrate surface than on the untreated substrate surface. The deposited particles on the treated substrate surface formed a layer as the deposition time increased to 120 min. The difference in the number concentration of particles deposited on both substrates can be expressed in a qualitative electrostatic aspect. This indicates that the electrostatic or trapped charge (from the electrosprayed particles) could not remain on the conductor surface permanently. If the trapped charge is positive, the free electron on the surface of the substrate will diffuse to the deposited particles until an equilibrium is achieved, in accordance with Fick's law. In addition, the charge dissipation mechanism also obeyed Ohm's law because the dielectric constant and surface resistivity of both substrates were different. The application of other mechanisms maybe necessary since a highly hydrophilic surface area will form a water layer inducing the hydrophilic interaction between particles (surfactant) and the substrate surface through the P–O network.

4. Conclusions

The effect of the chemical treatment of a substrate on the deposition of aerosol (TiO_2) particles derived from electrosprayed suspension droplets was demonstrated. A chemical treatment for modifying the (aluminum) substrate surface was found to be useful for promoting TiO_2 particle deposition. A treated substrate with an oxide layer was able to hold the deposited particles on the surface compared with an untreated substrate surface. By comparison with the untreated surface, it was considered that the adhesion force contributing to a high number concentration of particles deposited on the treated substrate originated from the hydrophilic interaction of the P–O network.

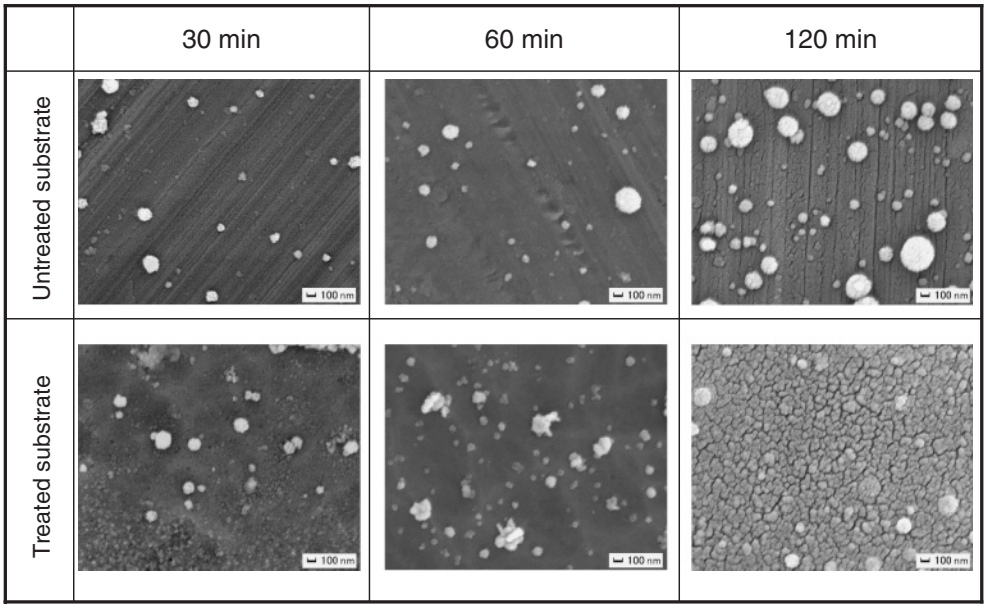

Fig. 7. Morphologies of electrosprayed TiO_2 particles (with supplying flow rate of 1.2 mL/h) prepared at different deposition times on the treated substrate (top) and the chemically treated substrate (bottom).

Acknowledgements

The authors are grateful to Dr. Mayumi Tsukada for her valuable advice, Masao Gen for the preparation of analysis equipment, and KAKOU Co., Ltd., Tokyo for providing the TiO_2 suspension. This study was supported in part by Special Condition Funds for Promoting Science and Technology from the Japan Science and Technology Agency, Grants-in-Aid for Scientific Research from the Japan Society for the Promotion of Science, and Grants-in-Aid for Scientific Research on Innovative Areas from the Ministry of Education, Culture, Sports, Science and Technology.

1) V. Meille: Appl. Catal. A **315** (2006) 1.
2) A. Jaworek and A. T. Sobczyk: J. Electrostat. **66** (2008) 197.
3) R. P. A. Hartman, D. J. Brunner, D. M. A. Camelot, J. C. M. Marijnissen, and B. Scarlett: J. Aerosol Sci. **30** (1999) 823.
4) N. Felitsyn, M. Peschke, and P. Kebarle: Int. J. Mass Spectrosc. **219** (2002) 39.
5) U. H. Verkerk and P. Kebarle: J. Am. Soc. Mass Spectrom. **16** (2005) 1325.
6) I. W. Lenggoro, H. Widiyandari, C. J. Hogan, Jr., P. Biswas, and K. Okuyama: Anal. Chim. Acta **585** (2007) 193.
7) I. W. Lenggoro, H. M. Lee, and K. Okuyama: J. Colloid Interface Sci. **303** (2006) 124.
8) P. Kebarle and L. Tang: Anal. Chem. **65** (1993) 972A.
9) M. Polat, H. Polat, and S. Chander: J. Aerosol Sci. **31** (2000) 551.
10) T. J. Krinke, H. Fissan, K. Deppert, M. H. Magnusson, and L. Samuelson: Appl. Phys. Lett. **78** (2001) 3708.
11) U. H. Verkerk and P. Kebarle: J. Am. Soc. Mass Spectrom. **16** (2005) 1325.
12) S. You and M. Choi: J. Aerosol Sci. **38** (2007) 1140.
13) G. Olanya, J. Iruthayaraj, E. Poptoshev, R. Makuska, A. Vareikis, and P. M. Claesson: Langmuir **24** (2008) 5341.
14) D. Jeon, C. Kim, J. M. Son, N. J. Lee, C. J. Kang, and Y. S. Kim: Jpn. J. Appl. Phys. **45** (2006) 513.
15) C. J. Kang, G. H. Buh, S. Lee, C. K. Kim, K. M. Mang, C. Im, and Y. Kuk: Appl. Phys. Lett. **74** (1999) 1815.
16) D. Schaadt, E. Yu, S. Sankar, and A. Berkowitz: Appl. Phys. Lett. **74** (1999) 472.
17) J. T. Jones, P. M. Bridger, O. J. Marsh, and T. C. McGill: Appl. Phys. Lett. **75** (1999) 1326.
18) M. S. Jean, S. Hudlet, C. Guthmann, and J. Berger: Phys. Rev. B **56** (1997) 15391.
19) S. Cunningham, I. A. Larkin, and J. H. Davis: Appl. Phys. Lett. **73** (1998) 123.
20) G. H. Buh, H. J. Chung, and Y. Kuk: Appl. Phys. Lett. **79** (2001) 2010.
21) R. P. A. Hartman, D. J. Brunner, D. M. A. Camelot, J. C. M. Marijinissen, and B. Scarlett: J. Aerosol Sci. **31** (2000) 65.
22) A. M. Gañán-Calvo: J. Aerosol Sci. **30** (1999) 863.
23) M. Adachi, K. Okuyama, and Y. Kousaka: J. Chem. Eng. Jpn. **16** (1983) 229.
24) M. Adachi, K. Okuyama, Y. Kousaka, H. Kozuru, and D. Y. H. Pui: Aerosol Sci. Technol. **11** (1989) 144.
25) I. W. Lenggoro, B. Xia, K. Okuyama, and J. F. de la Mora: Langmuir **18** (2002) 4584.
26) D. R. Chen, D. Y. H. Pui, and S. L. Kaufman: J. Aerosol Sci. **26** (1995) 963.
27) W. N. Wang, W. Widiyastuti, I. W. Lenggoro, T. O. Kim, and K. Okuyama: J. Electrochem. Soc. **154** (2007) J121.
28) A. Casu, P. C. Ricci, and A. Anedda: J. Raman Spectrosc. **40** (2009) 1224.
29) S. Balaji, Y. Djaoued, and J. Robichaud: J. Raman Spectrosc. **37** (2006) 1416.
30) M. L. Doche, J. J. Rameau, R. Durand, and F. Novel-Cattin: Corros. Sci. **41** (1999) 805.
31) H. Lu, C. Chen, H. Sun, X. Hu, and D. Yang: Ceram. Int. **31** (2005) 481.
32) M. Schacht, N. Boukis, and E. Dinjus: J. Mater. Sci. **35** (2000) 6251.
33) V. Burokas, A. Martushene, G. Bikul'chyus, and A. Ruchinskene: Russ. J. Appl. Chem. **82** (2009) 1835.
34) L. Y. Niu, Z. H. Jiang, G. Y. Li, C. D. Gu, and J. S. Jian: Surf. Coat. Technol. **200** (2006) 3021.
35) M. Rokita, M. Handke, and W. Mozgawa: J. Mol. Struct. **555** (2000) 351.
36) P. Kim, S. C. Jones, P. J. Hotchkiss, J. N. Haddock, B. Kippelen, S. R. Marder, and J. W. Perry: Adv. Mater. **19** (2007) 1001.
37) R. Sharma, S. Trigwell, A. S. Biris, R. A. Sims, and M. K. Mazumder: IEEE Trans. Ind. Appl. **39** (2003) 87.